

Impulsive-stimulated-scattering study of the normal-incommensurate phase transition in $[\text{N}(\text{CH}_3)_4]_2\text{ZnCl}_4$

Scott M. Silence and Keith A. Nelson

Department of Chemistry, Massachusetts Institute of Technology, Cambridge, Massachusetts 02139

Jacques Berger

Groupe de Physique des Solides, Université Paris 7—Université Paris 6, 75251 Paris CEDEX 05, France

(Received 25 October 1991)

The longitudinal acoustic anomaly along the a axis of the crystal $[\text{N}(\text{CH}_3)_4]_2\text{ZnCl}_4$ has been investigated near the normal-incommensurate (N -IC) phase transition temperature by impulsive stimulated scattering, for acoustic frequencies in the range of 350 MHz to 4 GHz. Considerable dispersion is seen over this frequency range. The major contribution to the anomaly below the N -IC transition is due to coupling to the amplitude mode, whose wave-vector-independent relaxation time τ diverges as the transition temperature T_i is approached with the temperature dependence given by $\tau = \tau_0 T_i / (T_i - T)$, with $\tau_0 \approx 0.6$ ps. We find no evidence for the coupling of the acoustic mode to the phase mode. The critical exponents that describe the order-parameter behavior have values consistent with mean-field theory. Critical-exponent values for other universality classes, particularly for the three-dimensional Ising model are found to be inconsistent with the data. The acoustic anomaly above T_i can be accounted for by the coupling of the longitudinal acoustic mode to energy-density fluctuations associated with the soft mode. A possible explanation for suppression of critical behavior in the acoustic anomaly near the N -IC transition is given.

I. INTRODUCTION

In recent years much attention has been focused on the class of compounds which undergo a phase transition (upon cooling) from a high-temperature normal (N) or “disordered” phase to an incommensurate (IC) phase at a temperature T_i , in which the crystal has acquired a spatial modulation along one or more of the crystallographic axes which is not a rational fraction of the N -phase lattice spacing. At some lower temperature T_l , another phase transition usually occurs and the additional modulation becomes commensurate with (“locks into”) the lattice periodicity. Tetramethylammonium tetrachlorozincate ($[\text{N}(\text{CH}_3)_4]_2\text{ZnCl}_4$ or TMATC-Zn) belongs to a large family of A_2MX_4 compounds that all exhibit IC phases.¹ In the high-temperature N phase, the crystal is orthorhombic (axis convention $c < a < b$), belonging to the space group D_{2h}^{16} ($Pman$). The N -IC transition in TMATC-Zn occurs at $T_i \approx 298$ K, and the transition to a ferroelectric commensurate (C) phase occurs at $T_l \approx 281$ K. There is an additional transition at $T_e \approx 277$ K from the ferroelectric phase to a ferroelastic phase.

The prototype (displacive) N -IC transition for this family of crystals behaves as follows. Approaching the N -IC phase transition from above, there are two degenerate soft phonons with opposite wave vectors whose absolute values are irrational in units of the reciprocal-lattice vectors of the N phase. The origin of the instability that gives rise to these soft modes is competition between various short-range forces in the crystal. Below T_i the two soft phonons transform into two new modes, an amplitude and phase modes. The amplitude mode behaves for

$T \rightarrow T_i$ like the soft-phonon mode above T_i , while the frequency of the phase mode behaves like that of an acoustic phonon (ω proportional to q), although the attenuation of this mode resembles that of an optic mode. In the case of TMATC-Zn, however, an order-disorder rather than displacive transition is believed to occur. Evidence for this comes from inelastic neutron scattering² and also from the failure to observe an underdamped amplitude mode in the IC phase using Raman-scattering techniques.³

The dynamics of the N -IC phase transition in TMATC-Zn have been investigated previously by probing acoustic anomalies with both ultrasonic techniques^{4,5} and Brillouin scattering.^{6,7} The acoustic strain S is coupled to the order parameter Q of the transition to lowest order by terms of the form SQ^2 in the free energy, as bilinear terms are symmetry forbidden. Although the acoustic anomalies are weak, they exhibit pronounced dispersion. In particular, the anomaly in the C_{11} elastic constant measured at ultrasonic frequencies (10–70 MHz) appears to be quite sharp, but measured at Brillouin-scattering frequencies (10 GHz) it is almost completely smoothed out. This indicates that relaxation of the order parameter (i.e., soft mode), which couples to the acoustic phonon, occurs on an intermediate time scale (100 ps to 10 ns) near T_i . This behavior is found for some other crystals in the A_2MX_4 family such as Rb_2ZnCl_4 , but not for others such as K_2SeO_4 , which exhibits very little dispersion in this frequency range.¹

In this investigation the longitudinal-acoustic modes propagating along the a axis (the axis of the IC modulation) of TMATC-Zn at frequencies between 350 MHz

and 4 GHz are characterized through impulsive stimulated scattering (ISS). These frequencies fall between the ranges investigated by ultrasonics and Brillouin-scattering techniques. The goal is to elucidate the static and dynamical critical behavior and, if possible, to extract information about the phase-mode as well as the amplitude-mode behavior in the IC phase. ISS has been used previously to investigate structural phase transitions, which give rise to acoustic anomalies at these frequencies in other compounds,⁸⁻¹⁰ none of which exhibit incommensurate phases.

II. EXPERIMENTAL DETAILS

Impulsive stimulated scattering is a time-domain coherent spectroscopy that has been described in detail.¹¹ On femtosecond-to-microsecond or longer times scales, the technique permits optical generation and observation of phase-coherent material excitations whose time-dependent responses are recorded. The technique is illustrated in Fig. 1. Two ultrashort laser pulses are temporally and spatially overlapped in a sample, with an angle θ between them. These pulses form an optical interference pattern with spacing Λ given by

$$\Lambda = \frac{2\pi}{q} = \frac{\lambda}{2 \sin(\theta/2)}, \quad (1)$$

where λ and θ are, respectively, the wavelength of and angle between the excitation pulses inside the sample and q is the magnitude of the scattering (grating) wave vector. When the two pulses are incident on the front surface of the sample (as in the present experiment), factors of the refractive index cancel in Eq. (1) and the excitation wavelength and angle in air can be used to calculate q . The crossed pulses produce coherent acoustic phonons of wave vector $\pm q$ through excitation mechanisms described in the following section.

The response induced by the excitation pulses is monitored using a third variably delayed probe pulse incident at the phase-matching angle for coherent scattering. Measurement of the scattered intensity as a function of time delay between the excitation and probe pulses per-

mits determination of the temporal profile of the material excitations. Assuming that the temporal response of the induced excitation is slow compared with the pulse duration, the ISS intensity $I(q, t)$ is given by

$$I(\mathbf{q}, t) \propto |G^{\epsilon\epsilon}(\mathbf{q}, t)|^2, \quad (2)$$

where $G^{\epsilon\epsilon}(\mathbf{q}, t)$ is the Green's-function response of the dielectric constant due to the mode or modes which are coherently excited. The projection of the tensor quantity ϵ or $G^{\epsilon\epsilon}$ selected by the light polarizations is assumed in Eq. (2). Specific forms for a variety of modes have been discussed previously,¹¹ and forms for the acoustic phonons probed in this experiment will be discussed below.

The experiments were conducted using a system consisting of two Nd:YAG lasers,¹² which produce variably delayed excitation and probe pulses of 100 ps duration, at a repetition rate of 600 Hz. The excitation laser is Q switched, mode locked, and cavity dumped to produce a single 1.064- μm pulse with approximately 1 mJ of energy. The probe laser is Q switched and mode locked, and one pulse in its output pulse train is selected electro-optically and frequency doubled to provide a 532-nm probe pulse. The timing between the excitation and probe pulses is controlled electronically by shifting the phase of a common mode-locker rf source to the probe laser and by electronically delaying the timing of the Q switches and single-pulse selector. This system offers several advantages over experimental systems in which the time delay is accomplished via a mechanical delay line. First, the time delay between excitation and probe pulses is no longer limited to the length of the mechanical delay line. Data can be recorded with delays up to 100 μs , which would correspond to a spatial delay of 33 km. This is important for measurement of low acoustic frequencies and attenuation rates. Second, changes in the probe-beam position and spot size at the sample due to delay line misalignment and beam divergence are eliminated. Third, increased energy is available for the excitation and probe pulses through the use of cavity dumping (for the excitation pulse) and two separate lasers. This is particularly important for observing modes with weak-scattering cross sections.

All of the experiments were carried out with the excitation and probe pulses and the signal polarized vertically relative to the scattering plane (VVVV) and with the wave vector q aligned along the a axis. Under these conditions longitudinal-acoustic (LA) modes aligned along the a axis (corresponding to the C_{11} elastic constant) were excited and probed. The experiments were carried out using scattering angles (in air) of 6.80°, 18.73°, 40.08°, and 88.33°. The excitation pulses were focused cylindrically to sizes of 2.5 mm (in the wave-vector direction) \times 0.1 mm. The large spot size minimizes uncertainty in q , which is important for measurement of weak acoustic attenuation rates, as has been discussed.¹¹ The pulse energies were kept below 200 μJ to avoid optical damage of the crystal. Data were recorded with sample temperatures between 320 and 250 K, always on cooling. The average cooling rates during the experiment were between 0.15 and 0.1 K per minute for temperatures less than 275 K and greater than 300 K, between 0.003 and

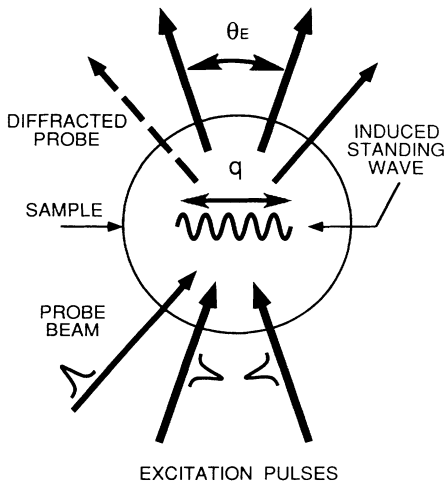


FIG. 1. Impulsive-stimulated-scattering (ISS) technique.

0.01 K per minute near T_i and in the IC phase above 290 K, and between 0.01 and 0.03 K per minute between 290 and 275 K. There was no detectable dependence of any of the data features on the cooling rate. Particular care was exercised in this regard because of the possible presence of domains in the IC phase, which can lead to artificially high acoustic attenuation rates.

The crystal was mounted in a vacuum chamber in contact with the cold finger of a closed-cycle helium refrigerator and a heater block, which was used to control the sample temperature. The temperature was recorded using a thermistor, which was in contact with the sample. The relative precision of the temperatures recorded in this experiment (the relative error between nominally identical temperatures recorded at different scattering wave vectors) is ± 0.1 K, as a result of the existence of temperature gradients in the sample. The absolute accuracy of the temperatures reported is ± 1 K.

Large ($\sim 6 \times 6 \times 6$ mm³) single crystals of TMATC-Zn were obtained by slow evaporation of a saturated solution at 40°C. The crystals used in these experiments were colorless, transparent, and free from visible defects except for several visible cleavage planes in the ab plane, which were caused by mechanical and thermal shocks which occurred during transportation from Paris, where the crystals were grown, to MIT. All laser beams were incident on the ab face of the crystal for the three lowest scattering angles and the ac face for the highest scattering angle. This was a consequence of the surface quality of the two different samples used at the different angles and has no effect on the measurement of the LA-phonon modes measured in the a direction.

III. ISS EXCITATION MECHANISMS

There are two distinct mechanisms through which the parallel-polarized excitation pulses can interact with the same to excite longitudinal-acoustic phonons. First, they can drive acoustic phonons directly through impulsive stimulated Brillouin scattering (ISBS). The equation of motion for acoustic waves in the crystal driven by this process is

$$\rho \frac{\partial^2 u_i}{\partial t^2} - \sum_{j,k,l} C_{ijkl} \frac{\partial^2 u_i}{\partial x_j \partial x_k} = - \sum_{i,k,l} \frac{1}{8\pi} \kappa_{klji} \frac{\partial}{\partial x_j} E_k E_l, \quad (3)$$

where ρ is the density, u_i is the local displacement in the i th direction, C_{ijkl} is the elastic constant tensor, E_i is the electric-field component in the i th direction, and $\kappa_{ijkl} = \partial \epsilon_{ij} / \partial S_{kl}$, where ϵ_{ij} is the dielectric tensor and S_{ij} is the acoustic strain given by

$$S_{ij} = \frac{1}{2} \left[\frac{\partial u_i}{\partial x_j} + \frac{\partial u_j}{\partial x_i} \right]. \quad (4)$$

The scattering geometry, pulse polarizations, and pulse durations chosen for this experiment limit the modes which are excited to longitudinal-acoustic phonons propagating along the a axis. For this case, Eq. (3) simplifies to

$$\rho \frac{\partial^2 u}{\partial t^2} - C \frac{\partial^2 u}{\partial x^2} = - \frac{1}{8\pi} \kappa \frac{\partial}{\partial x} E^2, \quad (5)$$

where all of the tensor subscripts have been dropped and u_x , C_{11} , κ_{1111} , and $E_y^2(x,t) \sim [1 + \cos(qx)]\delta(t)$, are assumed.

The solution to this wave equation yields

$$S(q,t) \propto \delta(q \pm q_0) G(q,t), \quad (6)$$

where q_0 , the excitation wave vector, is assumed to lie along the a axis and $S = S_{11}$ is the longitudinal strain along this axis. The Green's function response is

$$G(q,t) \propto \frac{q}{v} e^{-\gamma t} \sin(\omega t), \quad (7)$$

where ω and γ are the acoustic frequency and attenuation rate, respectively, and $v = \omega/q$ is the acoustic velocity.

The second mechanism through which the 1.06- μ m excitation pulses can excite longitudinal-acoustic phonons is by depositing heat into the sample through weakly allowed absorption into C-H vibrational overtones. This leads to thermal expansion, which causes both a steady-state thermal grating and a transient longitudinal-acoustic response. We refer to this process as impulsive stimulated thermal scattering (ISTS); other names have been used previously.¹⁴ In this case the acoustic strain is given by

$$S(q,t) \propto \delta(q \pm q_0) [e^{-\Gamma t} - e^{-\gamma t} \cos(\omega t)] \\ \approx \delta(q \pm q_0) [1 - e^{-\gamma t} \cos(\omega t)], \quad (8)$$

where the thermal diffusion rate Γ is negligibly slow on our experimental time scale.

The total dielectric response to impulsive stimulated Brillouin and thermal scattering is the sum of the Green's-function responses defined in Eqs. (7) and (8):

$$G^{\epsilon\epsilon}(q,t) = A e^{-\gamma t} \sin(\omega t) + B [1 - e^{-\gamma t} \cos(\omega t)], \quad (9)$$

where A and B reflect the relative amplitudes of the responses to ISBS and ISTS, respectively. The ISBS amplitude A is proportional to q [Eq. (7)], while the ISTS coefficient B is independent of q . Therefore the signal [given by Eq. (2)] at large scattering angles is dominated by ISBS and shows oscillations at 2ω , while the signal at small scattering angles is dominated by ISTS and shows oscillations at the fundamental frequency ω .

This treatment can be generalized by regarding the elastic constant C , not as a real number, but as a complex frequency-dependent inverse response function¹³ defined by

$$\sigma(\omega) = \tilde{C}(\omega) S(\omega), \quad (10)$$

where $\sigma = \sigma_1$ is the longitudinal stress along the a axis. This response function can be separated into real and imaginary parts:

$$\tilde{C}(\omega) = C_0 - \Delta C(\omega) = (C_0 - C') + iC'', \quad (11)$$

where C_0 is a real frequency-independent background

term and $\Delta C(\omega)$ is composed of the real and imaginary parts C' and C'' , respectively. In the analysis which follows, experimentally determined values of the acoustic frequency ω and attenuation rate γ which enter into Eq. (9) are expressed in terms of the real and imaginary parts of the elastic response function $C(\omega)$ through the relations

$$\omega = q \left(\frac{C_0 - C'}{\rho} \right)^{1/2}, \quad (12)$$

$$\gamma = -\frac{q^2 C''}{2\omega\rho}. \quad (13)$$

IV. RESULTS

A. Data features

Data taken at a scattering angle $\theta = 18.73^\circ$ (scattering wavelength $\Lambda = 3.269 \mu\text{m}$) are shown in Fig. 2 for crystal temperatures of 320 and 297 K. The data (solid curves) show oscillations at both the fundamental acoustic frequency ω and 2ω , indicating that both ISBS and ISTS mechanisms are active. Fits to the data (dashed curves) based on Eq. (9) are also shown, and the frequency $\nu = \omega/2\pi$ and attenuation rate γ obtained from the fits are shown for both temperatures. At 320 K the crystal is in the high-temperature orthorhombic (normal) phase, and the attenuation rate is quite small, but measurable. Note that the corresponding Brillouin linewidth $\gamma/2\pi$ of 0.9 MHz would be extremely difficult to measure by conventional methods. At 297 K, which is slightly below the normal-incommensurate phase-transition temperature, the attenuation rate has increased by approximately an order of magnitude, but the acoustic velocity has fallen by less than 1%. The complete temperature dependence of the acoustic parameters throughout the temperature range covered in this experiment is presented in Sec. IV B below.

There also exists the possibility that other light-scattering active relaxational modes, in particular the

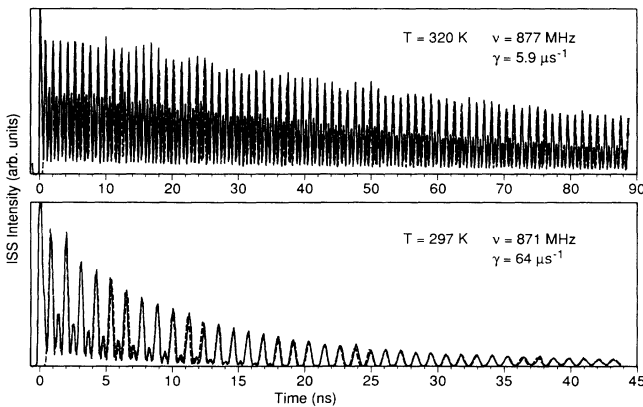


FIG. 2. ISS data taken with a scattering angle of $18^\circ 44'$ ($\Lambda = 3.269 \mu\text{m}$) at two sample temperatures. Solid lines are data, and dashed lines are fits to the data. Note the change in time scales between the scans.

phase mode, contribute to the data scans, but are effectively masked by the steady-state thermal grating. This can be ruled out through the wave-vector dependence of the relative intensity of the acoustic modes produced by the ISBS and ISTS mechanisms, which is illustrated in Fig. 3 for the three lowest angles used in this experiment. The ratio of the coefficients A and B defined in Eq. (9) is plotted as a function of q for the sample at $T = 300 \text{ K}$. Because of limitations in time resolution and the extremely high acoustic frequency at the highest wave vector (corresponding to a scattering angle $\theta = 88.33^\circ$), A/B could not be determined reliably at this wave vector. The points fall on a straight line, which extrapolates to a value quite close to $A/B = 0$ at $q = 0$. Any contributions to the signal from relaxational modes such as a phase mode (whose intensity should also be wave-vector dependent) would heterodyne with the acoustic signal and cause deviations from this linear relationship. Simulations indicate that signal from a phase mode with an intensity greater than 5% of the acoustic-mode intensity should be observable given the signal-to-noise ratio of the data. The linear relationship is obeyed over the entire temperature range covered by the experiment, indicating no additional contributions above this level to the signal.

B. Acoustic anomalies

The temperature-dependent velocity $v = \omega/q$ and attenuation rate γ of longitudinal acoustic phonons propagating along the a axis with wavelength $\Lambda = 3.269 \mu\text{m}$ are

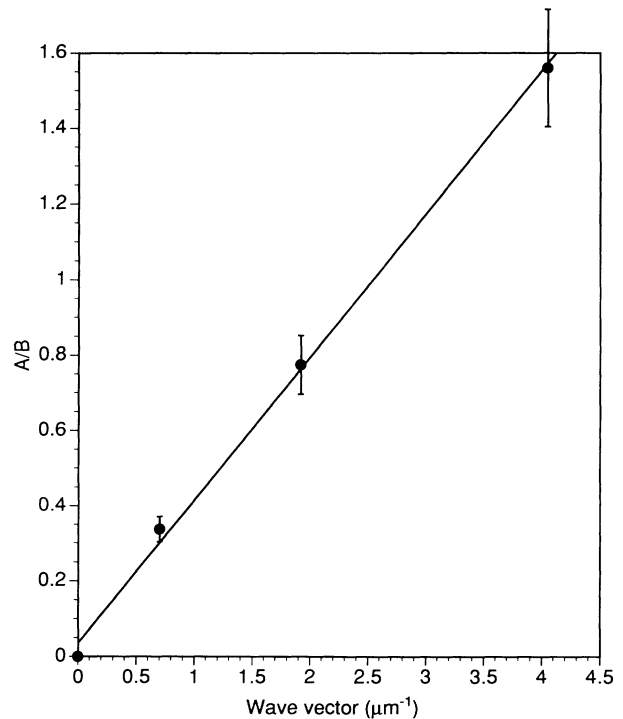


FIG. 3. Ratio of the amplitudes of the two acoustic-mode excitation mechanisms plotted vs acoustic wave vector. The points are described by a straight line.

shown in Fig. 4. The temperature range shown encompasses the N -IC phase transition at $T_i \approx 298$ K, the IC-C (ferroelectric) transition at $T_l \approx 281$ K, and the ferroelectric-to-ferroelastic transition at $T_e \approx 277$ K. These transitions, particularly the N -IC and the ferroelectric-to-ferroelastic transitions, are reflected in the anomalous acoustic behavior near them.

Figure 4 indicates that as the temperature is lowered from 320 K to T_i the attenuation rate increases from a temperature-independent background value, peaking slightly below T_i at 297 K. Upon further cooling the attenuation rate decreases, undergoing a slight increase again near the lock-in temperature T_l . A narrow peak in the attenuation rate, which has been suggested in previous ultrasonic data,⁵ occurs at T_e . Anomalous behavior in the acoustic velocity is also evident. The velocity increases gradually upon cooling until 305 K, at which point it begins to decrease gradually. This decrease becomes quite steep between 298 and 295 K, below which the velocity begins to increase again. It undergoes an abrupt increase at the first-order transition at T_e , as has been observed previously.⁵

As expected from previous Brillouin-scattering and ultrasonics results, the acoustic anomaly near T_i exhibits a strong dependence on the scattering wave vector q . This is illustrated in Fig. 5, which shows the acoustic attenuation rate scaled by the wave vector squared and the acoustic velocity over the range of scattering wavelengths investigated. The scattering wavelengths shown in Fig. 5 were corrected for small uncertainties in the values determined from Eq. (1) by assuming no dispersion in the velocity at 320 K and by assuming that the velocity determined at $\theta = 18.73^\circ$ is the true velocity. These wavelengths will be used for all subsequent data analysis. The attenuation rate at the largest wavelength could not be accurately determined because of noise in the data from parasitically scattered light, nor could the velocity be determined accurately at the smallest scattering wavelength because of small nonlinearities in the experimental time base, which are due to nonlinearities in the phase shifter described in the experimental section above. From Fig. 5(a) it can be seen that as the wave vector in-

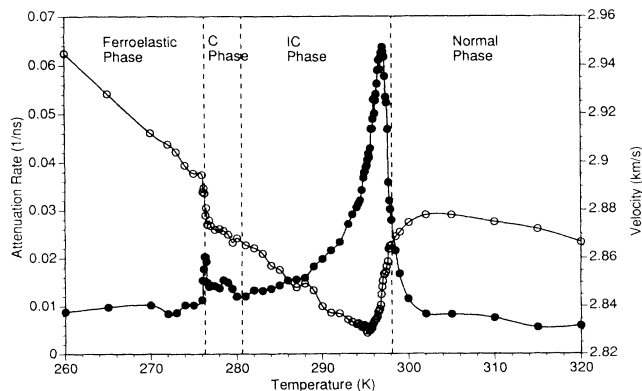


FIG. 4. Acoustic attenuation rate (solid circles) and velocity (open circles) shown as a function of temperature for $\Lambda = 3.269$ μm . The phases of the crystal are separated by dashed lines.

creases, the peak in the attenuation rate becomes considerably broader and shifts to lower temperatures. At the same time, the sharp drop in the acoustic velocity [Fig. 5(b)] becomes more gradual with increasing wave vector. These trends reflect the fact that in the hypersonic frequency range (300 MHz to 4 GHz) the condition $\omega\tau \ll 1$ is not fulfilled near the N -IC transition as it is at ultrasonic frequencies.

V. ANALYSIS OF ACOUSTIC ANOMALY NEAR T_i

In order to use the measured acoustic anomalies to quantitatively characterize the dynamics of the N -IC phase transition, it is necessary to relate the real and imaginary parts of the response function C [Eqs. (10)–(13)] to the dynamics that control the phase transition. As mentioned earlier, the lowest-order coupling between the strain S and order parameter Q takes the form SQ^2 . The leading terms in the Landau free-energy expansion are

$$F = F_0 + \frac{1}{2}AQ^2 + \frac{1}{4}BQ^4 + \frac{1}{6}DQ^6 + \frac{1}{2}C_0S^2 - \frac{1}{2}hSQ^2. \quad (14)$$

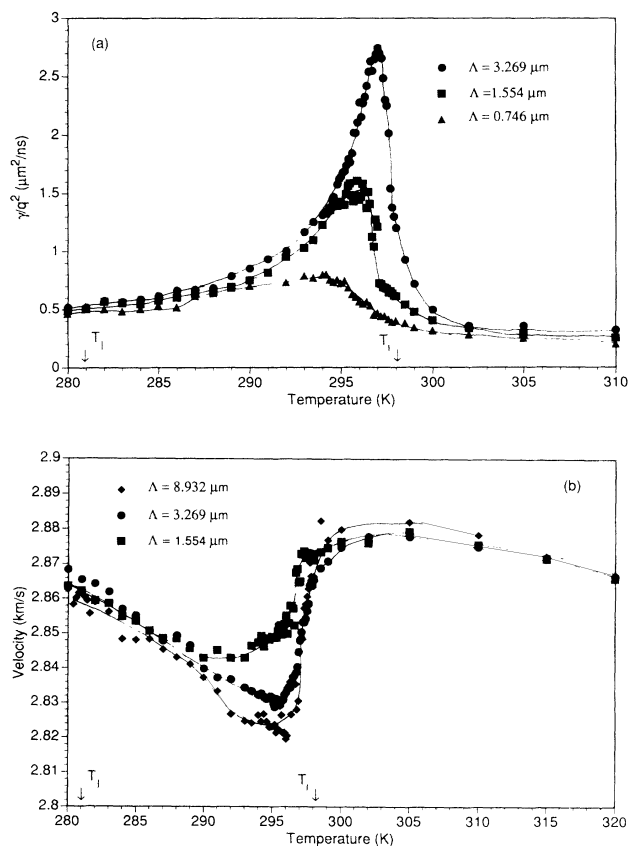


FIG. 5. (a) Acoustic attenuation rate γ scaled by q^2 shown as a function of temperature for the three scattering wavelengths at which γ could be determined accurately (lines are guides to the eye). Note the broadening of the peak and its shift to lower temperatures as Λ is decreased. (b) Acoustic velocity v shown as a function of temperature for the three scattering wavelengths at which v could be determined accurately. As Λ is decreased, the drop in the acoustic velocity becomes more gradual and less pronounced.

The first term is a background term; the second through fourth terms describe the free energy associated with the N -IC phase transition, which has an order parameter Q ; the fifth term is the free energy due to strain; and the last term is the coupling term with coupling constant h . The coefficient A is assumed to vary with temperature as $A = A_0(T - T_i)$, and all other coefficients are assumed to be temperature independent. The complex frequency-dependent elastic constant $C(\omega)$ defined in Eq. (10) can be obtained from this free energy expansion by

$$\tilde{C}(\omega) = \frac{\partial \sigma}{\partial S}, \quad (15)$$

where fluctuations in the stress defined by $\sigma = \partial F / \partial S$ are given by the equation

$$\delta \sigma = C_0 \delta \epsilon - h Q_0 \delta Q - \frac{1}{2} h (\delta Q)^2, \quad (16)$$

where Q_0 is the average value of the order parameter. Equation (14) and (16) indicate several temperature-dependent effects on the elastic susceptibility C . In the high- T phase, $Q_0 = 0$ and only the fluctuation term $(\delta Q)^2$ influences C . In the low- T phase, Q_0 is finite and both the $Q_0 \delta Q$ and fluctuation terms contribute to the susceptibility. Sufficiently far below T_i , the $(\delta Q)^2$ term can usually be neglected, and the Landau-Khalatnikov (LK) contribution due to the term $Q_0 \delta Q$ dominates.

The obvious asymmetry of the acoustic data (shown in Fig. 5) about T_i is due to the fact that both LK and fluctuation terms contribute to the anomalies below T_i , and only fluctuations contribute to the anomalies above T_i . Previously measured acoustic anomalies in IC crystals^{15,16} have been analyzed by first fitting the data above T_i with the fluctuation contribution and then, using the parameters determined from the analysis, subtracting the fluctuation contribution from the data below T_i and fitting the remaining data with the LK contribution. In the present case the anomalies above T_i are significantly smaller than those below T_i , and unique analysis of the data above T_i is difficult. Therefore the acoustic anomalies below T_i will first be analyzed using only the LK contribution. The question of the fluctuation contribution to the data, both above and below T_i , will be returned to below.

A. Landau-Khalatnikov contribution

Linearizing Eq. (16) with respect to δQ and considering order-parameter relaxation characterized by a relaxation time τ yields the following expression for $C(\omega)$ for $T < T_i$:

$$\tilde{C}(\omega) = C_0 - \frac{h^2 / (2B + 4DQ_0^2)}{1 - i\omega\tau}. \quad (17)$$

For $T > T_i$, $C(\omega) = C_0$. A detailed derivation of Eq. (17) is given in Ref. 13. This equation is valid whether the order parameter is assumed to be purely relaxational or a damped harmonic oscillator, provided its natural frequency ω_0 exceeds the acoustic frequency ω .

Combining Eq. (17) with Eqs. (12) and (13) leads to the classical LK expressions for the acoustic velocity v and

attenuation rate γ for $T < T_i$:

$$v = v_0 \left[1 - \frac{\Delta'}{1 + \omega^2 \tau^2} \right] \approx v_0 \left[1 - \frac{\Delta'}{1 + \bar{\omega}^2 \tau^2} \right], \quad (18)$$

$$\gamma = \gamma_0 + \omega \Delta' \frac{\omega \tau}{1 + \omega^2 \tau^2} \approx \gamma_0 + \bar{\omega} \Delta' \frac{\bar{\omega} \tau}{1 + \bar{\omega}^2 \tau^2}, \quad (19)$$

where v_0 and γ_0 are the values of the velocity and attenuation rate in the absence of the transition and Δ' is a unitless parameter given by

$$\Delta' = \frac{\Delta}{2\rho v_0^2} = \frac{1}{2\rho v_0^2} \frac{h^2}{2B + 4DQ_0^2}. \quad (20)$$

Since the acoustic frequency changes by about 2% near the N -IC transition, the average value of ω , denoted by $\bar{\omega}$, has been used in Eqs. (18) and (19). Further, Δ' is assumed to be independent of temperature (which will be discussed further below), and τ is assumed to have a temperature dependence given by

$$\tau = \tau_0 \left[\frac{T_i}{T_i - T} \right]^\rho, \quad (21)$$

where ρ is a dynamical critical exponent which is assumed to be 1. Deviations from this value will be discussed below.

Before the acoustic anomalies can be analyzed quantitatively, the transition temperature T_i must be determined. Within the framework of LK theory, it can be shown that, by setting

$$\left. \frac{\partial \gamma}{\partial T} \right|_{T=T_m} = 0, \quad (22)$$

the temperature T_m at which the maximum in the acoustic attenuation occurs is a linear function of the acoustic frequency, given by the equation

$$T_m = -(\tau_0 T_i) \omega + T_i. \quad (23)$$

A plot of T_m vs acoustic frequency at that temperature is shown in Fig. 6. A fit to these points using Eq. (23) is also shown. The transition temperature determined from this fit is $T_i = 298.0 \pm 0.1$ K. T_i will be fixed at this value for the remainder of the data analysis. It should be noted that the contribution to the data due to energy-density fluctuations, which will be addressed below, has been shown to have very little effect on the position of the attenuation maximum below T_i , and therefore the value of T_i determined from considering only the LK contribution should still be essentially correct in the presence of fluctuations.¹⁷ This will be confirmed below.

In order to apply Eqs. (18) and (19) to the data, it is necessary to fix the background attenuation rate γ_0 and velocity v_0 . The wave-vector dependence of γ_0 can be divided out by expressing γ_0 as γ'_0/q^2 . The value of γ'_0 will be fixed at $1.6 \times 10^{-3} \mu\text{m}^2/\text{ns}$ for all scattering wave vectors and temperatures, both above and below T_i . Fixing the velocity background is more problematic, since neither the frequency range nor temperature range investigated above T_i is large enough to permit an unambiguous

TABLE I. Parameters for the LK fits to the data for $T < T_i$ without the contribution from the fluctuation term.

Λ (μm)	ν (GHz)	τ_0 (ps)	Δ'
0.746	3.83 ^a	0.63 \pm 0.13	0.021 \pm 0.001
1.554	1.83 ^a	0.56 \pm 0.13	0.022 \pm 0.001
3.269	0.871 ^a	0.51 \pm 0.13	0.022 \pm 0.001
8.932	0.316 ^a	1.13 \pm 0.43	0.024 \pm 0.001
282 ^a	0.010	0.71	(0.022) ^b

^aValue at the attenuation maximum.

^bQuantity kept fixed.

frequency at the maximum of the acoustic attenuation. From the fit to the data shown in Fig. 6, a value of $\tau_0=0.64\pm 0.05$ ps is obtained for this relaxation time, which is consistent with the values shown in Table I.

Deviations from classical behavior in the LK contribution to include the effect of static critical behavior have been derived through dynamic scaling arguments¹⁸ and yield, for the acoustic anomalies,

$$v = v_0 [1 - \Delta' t_r^{2\beta-\gamma} G(\bar{\omega}\tau, \gamma)], \quad (25)$$

$$\gamma = \gamma_0 + \bar{\omega} \left[\frac{\gamma}{z\nu} \right] \Delta' t_r^{2\beta-\gamma} (\bar{\omega}\tau) F(\bar{\omega}\tau, \gamma), \quad (26)$$

where t_r is the reduced temperature $(T - T_i)/T_i$, β and γ are usual critical exponents, and $G(\omega\tau, \gamma)$ and $F(\omega\tau, \gamma)$ are analytical approximations to the real and imaginary parts of the relaxation function

$$(1 - i\omega\tau)^{-\gamma/z\nu}, \quad (27)$$

which are given by the expressions

$$F(\omega\tau, \gamma) = \frac{z\nu}{\gamma} \frac{1}{\omega\tau} \sin \left[\frac{\gamma}{z\nu} \arctan(\omega\tau) \right] \times \{ \cos[\arctan(\omega\tau)] \}^{\gamma/z\nu}, \quad (28)$$

$$G(\omega\tau, \gamma) = \cos \left[\frac{\gamma}{z\nu} \arctan(\omega\tau) \right] \{ \cos[\arctan(\omega\tau)] \}^{\gamma/z\nu}. \quad (29)$$

Equations (28) and (29) give the correct behavior in the limiting cases of $\omega\tau \ll 1$ and $\omega\tau \gg 1$, and they satisfy the Kramers-Kronig relationship. In mean-field theory, $\beta=0.5$ and $\gamma=1$, and Eqs. (25) and (26) reduce to Eqs. (18) and (19).

Previous analysis of the acoustic anomalies at ultrasonic frequencies in Rb_2ZnCl_4 ,¹⁶ which is isomorphic to TMATC-Zn , have shown critical exponents consistent with three-dimensional (3D) Ising-model behavior ($\beta=0.324$ and $\gamma=1.24$). Fits to the $\Lambda=3.269 \mu\text{m}$ data using Eqs. (25), (26), (28), and (29) and assuming Ising-model values for the critical exponents are shown in Fig. 7 (dotted lines). The values for T_i and the attenuation rate and velocity backgrounds above T_i were fixed to the values discussed above, and the value of $z\nu$ was set to 1, which is consistent with conventional van Hove relaxation and is in agreement with previous measurements of

the critical behavior of IC crystals.^{15,16} The backgrounds below T_i were treated as fitting parameters, and τ_0 and Δ' were varied independently to fit the attenuation rate and velocity simultaneously. The fit to the attenuation rate using these exponent values is shown in Fig. 7(a), with the values of the parameters $\tau_0=0.91$ ps and $\Delta'=6.82 \times 10^{-4}$. In order to yield an adequate fit to the data, the attenuation background below T_i was found to be approximately twice that above T_i . This is an effect of the term $(t_r)^{2\beta-\gamma}$ in Eq. (26), which reduces the attenuation rate back to the background level for temperatures above T_i . This factor and the factor of γ also present in Eq. (26) reduce the value of Δ' well below the value determined from the mean-field fit. The fit to the acoustic velocity with the identical parameter values is shown in Fig. 7(b). This fit underestimates the magnitude of the anomaly and also has significant curvature in the velocity below T_i . The fit to the velocity is not very sensitive to the background velocity below T_i ; essentially identical fits are obtained by assuming either the background velocity of the mean-field fit [assumed in the fit shown in Fig. 7(b)] or assuming that the background below T_i has the same behavior as that above T_i .

It is evident from Fig. 7, particularly Fig. 7(b), that the assumption of 3D Ising behavior of the LK contribution to the acoustic anomaly yields significantly worse fits to the data using the assumed behaviors for the velocity and attenuation rate backgrounds than the fits assuming mean-field behavior for the LK contribution. In order to fit the data adequately with Ising values for the critical exponents, the backgrounds must be assumed to be different from the simplest possible behaviors discussed above. In particular, the attenuation rate must be assumed to have a background value below T_i of twice that above T_i . Although this cannot be completely ruled out, it seems unlikely.

B. Energy-density fluctuation contribution

The presence of acoustic anomalies above T_i and deviations from LK behavior for $\Delta T < 1$ K below T_i are due to the presence of fluctuations in the order parameter of order $(\delta Q)^2$ near the transition. Inclusion of this effect has been dealt with in a number of different ways for different IC crystals.¹³ The dynamical scaling approach of Fossum¹⁸ (discussed above for the LK contribution to the acoustic anomalies) will be adopted here to characterize the acoustic anomalies for $T > T_i$. Within this framework the anomalies in the acoustic velocity and attenuation rate due to energy-density fluctuations are given by the equations¹⁶

$$\Delta v = v_0 C t_r^{-\mu} (1 + D t_r^{0.5}) G(\bar{\omega}\tau^+, \mu), \quad (30)$$

$$\Delta \gamma = \left[\frac{\mu}{z\nu} \right] \bar{\omega} C t_r^{-\mu} (1 + D t_r^{0.5}) (\bar{\omega}\tau^+) F(\bar{\omega}\tau^+, \mu), \quad (31)$$

where C is a unitless coupling constant, μ is the critical

0.9. Using the results of both techniques together, which extends the dynamic range covered by either technique alone by nearly two orders of magnitude, yields a value of $\rho=0.97\pm 0.03$. This value corresponds to the slope of the dotted line shown in Fig. 8(a).

This determination of ρ assumes that the parameter Δ' is independent of temperature, which is not necessarily true [cf. Eq. (20)]. If $B \ll D$, where B and D are the coefficients which enter into the Landau expansion [Eq. (14)], Δ' has a temperature dependence given by $\Delta' \sim Q_0^2 \sim (-t_r)^{2\beta}$, where t_r is the reduced temperature given by $(T - T_i)/T_i$ and β is the static critical exponent. In this limit the temperature dependence of $(\gamma - \gamma_0)/q^2$ is given by $(\Delta T)^{-(1+2\beta)}$ (with $\Delta T = T_i - T$), and so the slope in Fig. 8(a) would be given by $-(1+2\beta)$. For smaller but still finite values of D/B , the leading-order corrections to the slope of Fig. 8(a) are of the form $-[1+2(D/B)2\beta]$ away from $\Delta T=0$. The fact that the tangent line to the $\omega\tau \ll 1$ data of Fig. 8(a) has a slope of nearly 1 indicates that Δ' is essentially independent of temperature for the range of ΔT covered in this experiment.

Figure 8(b) shows the values for the acoustic velocity $\Delta v = v - v_0$ plotted against ΔT on a log-log scale for acoustic modes with wavelengths $\Lambda = 8.932, 3.269,$ and $1.554 \mu\text{m}$. Although there is significant scatter in the data, it is evident that the LK fits adequately characterize

the data over most of the temperature range, with systematic deviations again occurring at values of $\Delta T < 1$ K.

The values for the parameters τ_0 and Δ' determined at all four wave vectors from the fits to the data are shown in Table I. The values of these parameters for $\Lambda = 3.269$ and $1.554 \mu\text{m}$ were obtained by consistent fits of both γ and v , while the parameters for $\Lambda = 0.746$ and $8.932 \mu\text{m}$ were obtained by fitting only the attenuation rate and velocity, respectively. The increased error bars on the parameters determined at the smallest and particularly the largest wavelengths reflect the fact that fitting only γ or v alone reduces the uniqueness of the fit. From Table I it is evident that there is no dependence of either τ_0 or Δ' on the acoustic wave vector within the assigned error bars. This conclusion is further reinforced by the results of ultrasonic experiments, which yielded a value of $0.56 \times 10^{-14} \text{ db cm}^{-1} \text{ Hz}^{-2} \text{ K}^{0.9}$ for a parameter B , which can be related to τ_0 via the equation

$$B = \frac{4\pi^2 T_i \Delta'}{8.686v} \tau_0. \quad (24)$$

Assuming that Δ' is independent of acoustic frequency, this yields a value of $\tau_0 = 0.71$ ps for the coefficient of the relaxation time which couples to a 10-MHz acoustic mode. This is also included in Table I.

The value of τ_0 can also be obtained from the slope of Eq. (23), which relates the temperature to the acoustic

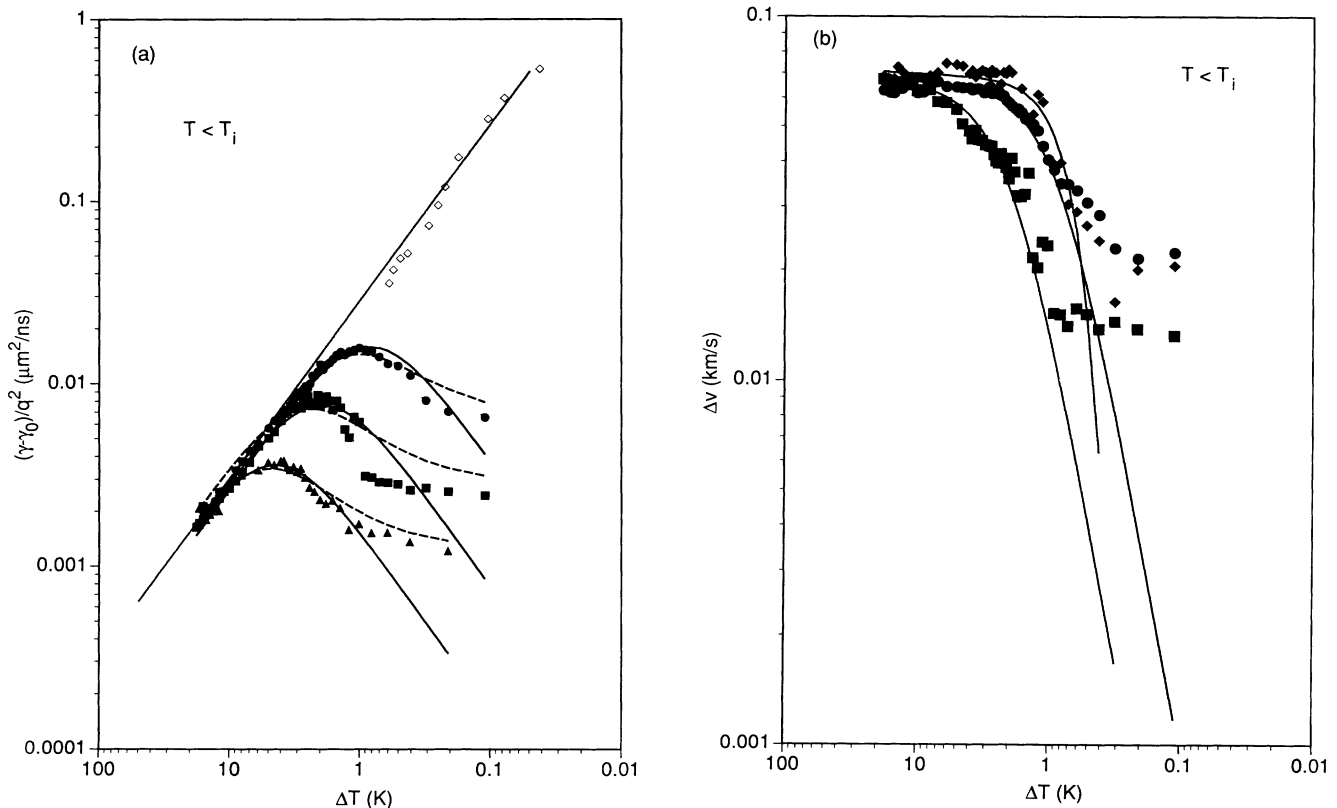


FIG. 8. (a) $(\gamma - \gamma_0)/q^2$ vs $\Delta T = T_i - T$ ($T < T_i$) for the data illustrated in Fig. 5(a) and the ultrasonics data of Ref. 4. The dotted line corresponds to $\omega\tau \ll 1$ and has a slope of 0.97 ± 0.03 . The solid lines are the LK fits to the data, with mean-field values for the static critical exponents. The dashed lines include contributions from the fluctuation term also. (b) $\Delta v = v - v_0$ vs ΔT ($T < T_i$) for the data illustrated in Fig. 5(b). The solid lines are the fits described in (a).

TABLE I. Parameters for the LK fits to the data for $T < T_i$ without the contribution from the fluctuation term.

Λ (μm)	ν (GHz)	τ_0 (ps)	Δ'
0.746	3.83 ^a	0.63 \pm 0.13	0.021 \pm 0.001
1.554	1.83 ^a	0.56 \pm 0.13	0.022 \pm 0.001
3.269	0.871 ^a	0.51 \pm 0.13	0.022 \pm 0.001
8.932	0.316 ^a	1.13 \pm 0.43	0.024 \pm 0.001
282 ^a	0.010	0.71	(0.022) ^b

^aValue at the attenuation maximum.

^bQuantity kept fixed.

frequency at the maximum of the acoustic attenuation. From the fit to the data shown in Fig. 6, a value of $\tau_0=0.64\pm 0.05$ ps is obtained for this relaxation time, which is consistent with the values shown in Table I.

Deviations from classical behavior in the LK contribution to include the effect of static critical behavior have been derived through dynamic scaling arguments¹⁸ and yield, for the acoustic anomalies,

$$v = v_0 [1 - \Delta' t_r^{2\beta-\gamma} G(\bar{\omega}\tau, \gamma)], \quad (25)$$

$$\gamma = \gamma_0 + \bar{\omega} \left[\frac{\gamma}{z\nu} \right] \Delta' t_r^{2\beta-\gamma} (\bar{\omega}\tau) F(\bar{\omega}\tau, \gamma), \quad (26)$$

where t_r is the reduced temperature $(T - T_i)/T_i$, β and γ are usual critical exponents, and $G(\omega\tau, \gamma)$ and $F(\omega\tau, \gamma)$ are analytical approximations to the real and imaginary parts of the relaxation function

$$(1 - i\omega\tau)^{-\gamma/z\nu}, \quad (27)$$

which are given by the expressions

$$F(\omega\tau, \gamma) = \frac{z\nu}{\gamma} \frac{1}{\omega\tau} \sin \left[\frac{\gamma}{z\nu} \arctan(\omega\tau) \right] \times \{ \cos[\arctan(\omega\tau)] \}^{\gamma/z\nu}, \quad (28)$$

$$G(\omega\tau, \gamma) = \cos \left[\frac{\gamma}{z\nu} \arctan(\omega\tau) \right] \{ \cos[\arctan(\omega\tau)] \}^{\gamma/z\nu}. \quad (29)$$

Equations (28) and (29) give the correct behavior in the limiting cases of $\omega\tau \ll 1$ and $\omega\tau \gg 1$, and they satisfy the Kramers-Kronig relationship. In mean-field theory, $\beta=0.5$ and $\gamma=1$, and Eqs. (25) and (26) reduce to Eqs. (18) and (19).

Previous analysis of the acoustic anomalies at ultrasonic frequencies in Rb_2ZnCl_4 ,¹⁶ which is isomorphic to TMATC-Zn , have shown critical exponents consistent with three-dimensional (3D) Ising-model behavior ($\beta=0.324$ and $\gamma=1.24$). Fits to the $\Lambda=3.269 \mu\text{m}$ data using Eqs. (25), (26), (28), and (29) and assuming Ising-model values for the critical exponents are shown in Fig. 7 (dotted lines). The values for T_i and the attenuation rate and velocity backgrounds above T_i were fixed to the values discussed above, and the value of $z\nu$ was set to 1, which is consistent with conventional van Hove relaxation and is in agreement with previous measurements of

the critical behavior of IC crystals.^{15,16} The backgrounds below T_i were treated as fitting parameters, and τ_0 and Δ' were varied independently to fit the attenuation rate and velocity simultaneously. The fit to the attenuation rate using these exponent values is shown in Fig. 7(a), with the values of the parameters $\tau_0=0.91$ ps and $\Delta'=6.82 \times 10^{-4}$. In order to yield an adequate fit to the data, the attenuation background below T_i was found to be approximately twice that above T_i . This is an effect of the term $(t_r)^{2\beta-\gamma}$ in Eq. (26), which reduces the attenuation rate back to the background level for temperatures above T_i . This factor and the factor of γ also present in Eq. (26) reduce the value of Δ' well below the value determined from the mean-field fit. The fit to the acoustic velocity with the identical parameter values is shown in Fig. 7(b). This fit underestimates the magnitude of the anomaly and also has significant curvature in the velocity below T_i . The fit to the velocity is not very sensitive to the background velocity below T_i ; essentially identical fits are obtained by assuming either the background velocity of the mean-field fit [assumed in the fit shown in Fig. 7(b)] or assuming that the background below T_i has the same behavior as that above T_i .

It is evident from Fig. 7, particularly Fig. 7(b), that the assumption of 3D Ising behavior of the LK contribution to the acoustic anomaly yields significantly worse fits to the data using the assumed behaviors for the velocity and attenuation rate backgrounds than the fits assuming mean-field behavior for the LK contribution. In order to fit the data adequately with Ising values for the critical exponents, the backgrounds must be assumed to be different from the simplest possible behaviors discussed above. In particular, the attenuation rate must be assumed to have a background value below T_i of twice that above T_i . Although this cannot be completely ruled out, it seems unlikely.

B. Energy-density fluctuation contribution

The presence of acoustic anomalies above T_i and deviations from LK behavior for $\Delta T < 1$ K below T_i are due to the presence of fluctuations in the order parameter of order $(\delta Q)^2$ near the transition. Inclusion of this effect has been dealt with in a number of different ways for different IC crystals.¹³ The dynamical scaling approach of Fossum¹⁸ (discussed above for the LK contribution to the acoustic anomalies) will be adopted here to characterize the acoustic anomalies for $T > T_i$. Within this framework the anomalies in the acoustic velocity and attenuation rate due to energy-density fluctuations are given by the equations¹⁶

$$\Delta v = v_0 C t_r^{-\mu} (1 + D t_r^{0.5}) G(\bar{\omega}\tau^+, \mu), \quad (30)$$

$$\Delta \gamma = \left[\frac{\mu}{z\nu} \right] \bar{\omega} C t_r^{-\mu} (1 + D t_r^{0.5}) (\bar{\omega}\tau^+) F(\bar{\omega}\tau^+, \mu), \quad (31)$$

where C is a unitless coupling constant, μ is the critical

exponent related to heat capacity, D is a parameter which accounts for leading-order corrections to scaling, τ^+ is the relaxation time of the energy-density fluctuations above T_i , and all other terms are defined above.

The anomalies in the acoustic attenuation rate and velocity for temperatures $T > T_i$ are plotted on a log-log scale in Fig. 9. The backgrounds assumed in Sec. V A have been subtracted from the data shown in Fig. 9. Figure 9(a) shows the data for the same scattering wave vectors which are shown in Fig. 8(a) for temperatures $T < T_i$, and Fig. 9(b) shows only data taken with $\Lambda = 3.269 \mu\text{m}$. The velocities at other wave vectors contained too much scatter to allow quantitative analysis. Equations (30) and (31) can be used to analyze the data, and the results are also shown in Fig. 9. For all of the fits carried out, the relaxation time τ^+ (which has a different value than the relaxation time τ for the LK contribution) was assumed to have the soft-mode behavior described by Eq. (21), T_i was fixed to 298.0 K, and the critical-exponent product $z\nu$ was assumed to be 1 (as above). The data could be fit adequately by assuming a broad range of values for the critical exponent μ . The choice $\mu = 0.11$, which corresponds to 3D Ising-model behavior, is shown in Fig. 9 (solid lines). These values are in agreement with those found for systems isomorphous to TMAZC-Zn above T_c .¹⁶ Although the Ising values for the critical exponents are not unique, they yield better fits than the

values for other models such as the XY model with the simplest choice of background velocities and attenuation rates assumed here. For these fits $\tau_0^+ = 0.8$ ps, $C = 1.3 \times 10^{-2}$, and $D = -2.5$. The fits to the acoustic attenuation rates [Fig. 9(a)] are quite good, but the fit to the acoustic velocity [Fig. 9(b)] consistently overestimates the magnitude of the anomaly, although the temperature dependence of the fit is roughly consistent with the data. A better fit to the data is obtained with the parameters $\tau_0^+ = 0.8$ ps, $C = 3.9 \times 10^{-3}$, and $D = -5.4$, which reduces the magnitude of the anomaly and increases its curvature at large values of ΔT [dashed line in Fig. 9(b)]. The fact that different parameters are needed to fit the anomaly in the acoustic velocity is most likely due to the difficulty of accurately subtracting the background velocity and cannot be taken as evidence of the inadequacy of the Ising-model fits. The best fits to the anomalies in the attenuation rate and velocity plotted on a linear scale with the background terms included for $\Lambda = 3.269 \mu\text{m}$ are also shown in Figs. 7(a) and 7(b).

As discussed above, the fluctuations in the energy density also contribute to the anomaly below T_i and should be included along with the LK contribution in the analysis of the data. Such an analysis is complicated by the fact that even accurate characterization of the fluctuation contribution above T_i does not uniquely determine the fluctuation contribution below T_i . Such an

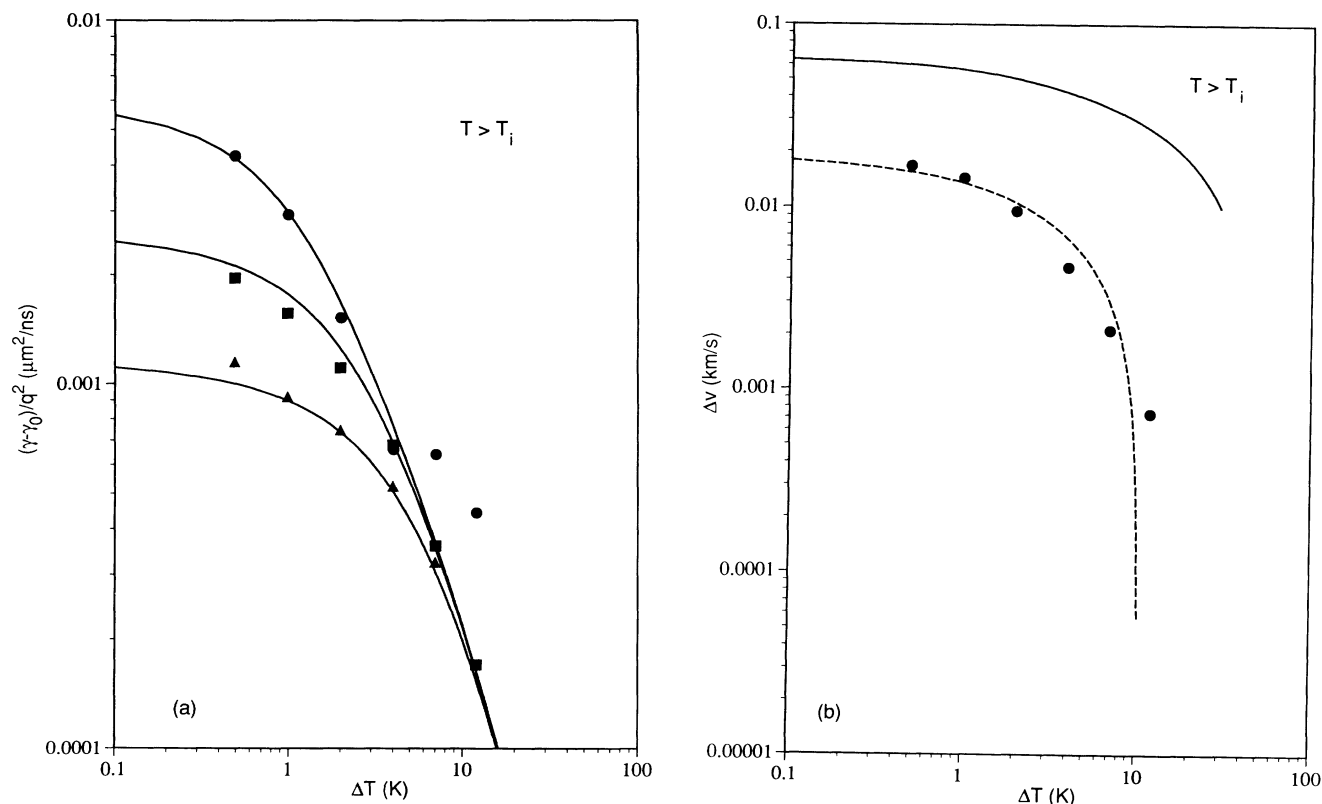


FIG. 9. (a) $(\gamma - \gamma_0)/q^2$ vs $\Delta T = T_i - T$ ($T > T_i$) for the data illustrated in Fig. 5(a). The lines are fits to the data due to energy-density fluctuations assuming a 3D Ising value for the critical exponent μ . (b) $\Delta v = v_0 - v$ vs ΔT ($T > T_i$) for the data with $\Lambda = 3.269 \mu\text{m}$. The solid line is the fit using parameters consistent with the attenuation rate fits, and the dashed lines uses the parameters described in the text.

analysis is even more difficult in the absence of accurate characterization of the fluctuation contribution above T_i . However, using reasonable assumptions regarding the fluctuation contribution below T_i , it is possible to assess the effect that this contribution has on the parameters of the dominant LK contribution. The first assumption is that the relaxation time of the energy-density fluctuations below T_i is given by $\tau_0^- = 0.5\tau_0^+$. This is consistent with classical van Hove behavior of the singularity at T_i , which has been assumed in the analysis of the data above ($z\nu=1$). It is also assumed that both the critical exponent μ and the magnitude of the correction to the scaling term D are the same above and below T_i . The final assumption regards the value of C , the magnitude of the contribution of the fluctuation term below T_i . We assume that the magnitude of the fluctuation contribution below T_i is equal to that above T_i . This is consistent with theoretical arguments that the universality class for the critical behavior of the N -IC transition is the $n=2$ Heisenberg (XY) model.¹⁹ For this model, $C(T < T_i) = 0.97C(T > T_i)$.¹⁶ Further, this assumption has been found to be adequate in the analysis of ultrasonic attenuation near the λ point in liquid helium,²⁰ which is of the same universality class. In that case a critical comparison was possible because of the fact that the transition temperature was accurately known and the temperature resolution of the experiment was in the μK range. Using these assumptions, the contribution to the anomaly in the attenuation rate due to energy-density fluctuations below T_i is shown in Fig. 7(a) for the scattering wavelength $\Lambda = 3.269 \mu\text{m}$.

With these assumptions for the parameters for the fluctuation contribution, the anomaly below T_i can be reanalyzed. The acoustic velocity is given by the sum of Eqs. (18) and (30), and the attenuation rate is given by the sum of Eqs. (19) and (31). The parameters in the fluctuation contribution are fixed at a given wave vector, and the LK parameters τ_0 and Δ' are allowed to vary. The resulting fits for the acoustic attenuation rates are shown in Fig. 8(a) (dashed lines). From Fig. 8(a) it is apparent that inclusion of the fluctuation contribution improves the fits to the data, although the fits overestimate the magnitude of the attenuation rate near T_i at all wave vectors. This may indicate that either the magnitude of the fluctuation term near T_i is less than assumed or there is a weak dependence of Δ' on temperature. The LK parameters for these fits are shown in Table II. The value of the parameter Δ' decreases by 10–20% and the value of τ_0 increases by 20–40% when the effect of fluctuations below T_i are included. Uncertainty in the background velocity near T_i coupled with the small change in velocity near this temperature prevents a quantitative analysis of the contribution of the fluctuation term to the acoustic velocity.

It should be mentioned that assuming a value for C which is larger below T_i than above, such as a value of $C(T < T_i) = 1.85C(T > T_i)$ predicted by the Ising model,¹⁶ causes the attenuation rate to drop below zero over the temperature range from 297.5 K to T_i . This is unphysical, and therefore such values of C below T_i can be

TABLE II. Parameters for the LK fits to the data for $T < T_i$ including the contribution from the fluctuation term described in the text.

Λ (μm)	ν (GHz)	τ_0 (ps)	Δ'
0.746	3.83 ^a	0.75±0.13	0.019±0.001
1.554	1.83 ^a	0.77±0.13	0.019±0.001
3.269	0.871 ^a	0.70±0.13	0.017±0.001

^aValue at the attenuation maximum.

ruled out. This may indicate that the fact that Ising-model exponents were found to yield adequate fits to the data above T_i is misleading and that the velocity and attenuation rate backgrounds are more complicated than assumed in this analysis. It is also possible that the correct theoretical model for this phase transition is not fully understood. As a final note, subtraction of the contribution to the anomaly in the attenuation rate does not change the position of the attenuation maximum by more than 0.1 K at any of the wave vectors investigated in this experiment. Therefore the transition temperature determined in the beginning of Sec. V A remains unchanged within the assigned error bars in the presence of fluctuations.

VI. DISCUSSION

A. Mean-field behavior of critical exponents

Over most of the temperatures range below T_i , the acoustic anomalies in TMatC-Zn are described quantitatively by the Landau-Khalatnikov contribution to the anomaly. Assuming that there is no excess acoustic attenuation for temperatures less than T_i and that the background velocity is linear in temperature (with a discontinuity in the slope allowed at T_i), the critical exponents are found to be those of mean-field theory. To describe these exponents by those of other universality classes, such as the 3D Ising model, would require both a large excess attenuation below T_i and a substantial curvature in the background velocity, neither of which is justified. The present experiment thus yields determinations of the critical exponents associated with the N -IC transition in TMatC-Zn.

The static critical exponent values are in contrast with the values of the critical exponents reported for materials isomorphic to TMatC-Zn,¹³ particularly those determined through ultrasonic techniques in RbZnCl₄.¹⁶ There are several possible reasons for this discrepancy. The first is that the focus of the ultrasonic measurements was on the fluctuation term above T_i . The critical exponents for this contribution to the acoustic anomaly could not be established in the present experiment, but were consistent with those of the Ising model as well as mean-field theory. The exponents for the LK contribution near T_i in the ultrasonics data were assumed to be those of the Ising model, but the uniqueness of this identification was not explored.

The second possible reason for the difference of the measured critical exponents between these two experi-

ments is that non-mean-field behavior obtains over a narrower temperature range in TMATC-Zn than in RbZnCl₄ and therefore cannot be observed in the present experiment. This may be due to a suppression of the acoustic anomaly in TMATC-Zn, especially further below T_i where the anomalies are strongest in the present experiment. The two crystals have very similar properties. The N -IC transitions are both of the order-disorder variety and involve rotations of the ZnCl₄ tetrahedra. Both of the materials undergo a lock-in transition which also involves rotations of these tetrahedra and which results in an improper ferroelectric phase with the direction of polarization along the c axis (with the convention $b > a > c$). The temperature range over which the IC phase is stable in RbZnCl₄ is approximately 110°, which is much larger than the range for TMATC-Zn (approximately 17°). It is possible that the coupling of the acoustic mode to the polarization mode in the IC phase suppresses the critical fluctuations, even into the IC phase, since the same types of motions give rise to the two transitions. This would have a much more pronounced effect on the N -IC transition in TMATC-Zn because of the much smaller temperature difference between the N -IC and lock-in transitions.

B. Amplitude- and phase-mode couplings

Throughout the analysis both the LK relaxation time τ and the fluctuation relaxation time τ^+ have been assumed to have the temperature dependence given by Eq. (21). Above T_i the relaxation time τ^+ is identified with the (degenerate) soft-mode energy-relaxation time. Below T_i this degeneracy is lifted, and the relaxation time τ can be associated with either the amplitude mode, phase mode, or both. If relaxation is due primarily to the acousticlike phase mode, its rate should be dependent on the wave vector of the acoustic mode, increasing as the acoustic wave vector is decreased. If the relaxation is due primarily to the opticlike amplitude mode, the relaxation time should be independent of the acoustic wave vector. From Table I it can be seen that, within the error of the experiment, τ is independent of q . Therefore we attribute the observed acoustic anomaly to coupling with the amplitude mode. It should be noted that the wave-vector dependence of the relaxation time associated with the phase mode may be altered by pinning of this mode at $q=0$, which would make the relaxation time relatively wave-vector independent for small values of q .

This result is also consistent with the reported Brillouin-scattering data. Equation (21) and the wave-vector-independent value of τ measured in the present experiment indicate a peak in the acoustic attenuation for $T < T_i$ at $T_m \approx 287.5$ K for an acoustic frequency of 9 GHz. This is qualitatively what is observed.⁷ It has been suggested⁷ that the apparent lack of a sharp acoustic anomaly at Brillouin-scattering frequencies is due to masking of the anomaly by coupling of the acoustic mode to the phase mode. No evidence is found for such a coupling in this experiment.

There exists very little independent information on either the amplitude or phase mode with which to compare

the results of these experiments. Temperature-dependent low-frequency Raman-scattering results³ revealed no strongly temperature-dependent low-frequency modes in the IC phase, indicating that these modes are most likely overdamped or relaxational in this phase. NMR results²¹ have indicated similar behavior, as well as a gap in the phase mode of $\sim 10^{11} - 10^{12} \text{ s}^{-1}$.

Direct probing of the amplitude and phase modes in the IC phase was attempted on both picosecond and femtosecond time scales using ISS. Direct observation of soft-optic-phonon modes have been reported recently in the materials KNbO₃ (Ref. 22) and BaTiO₃.²³ Although the relaxation times are on the correct time scale for direct probing to be successful in TMATC-Zn, no soft modes were observed. This is due most likely to the relative weakness of the scattering cross sections for these modes.

VII. CONCLUSIONS

The longitudinal-acoustic anomaly along the a axis of the crystal TMATC-Zn has been investigated near the normal-incommensurate (N -IC) phase transition by impulsive stimulated scattering for acoustic frequencies in the range of 350 MHz to 4 GHz. Considerable dispersion is seen over this frequency range. Below the N -IC transition, the major contribution to the anomaly is due to relaxation of the order parameter (Landau-Khalatnikov contribution). The relaxation time is adequately characterized by a single wave-vector-independent relaxation time with the temperature dependence given by $\tau = \tau_0 T_i / (T_i - T)$, with $\tau_0 \approx 0.6$ ps. This is consistent with the relaxation time measured with ultrasonics techniques. We identify this relaxation as the amplitude mode and find no evidence for the coupling of the acoustic mode to the phase mode. The previously measured Brillouin-scattering data are also seen to be qualitatively explained with the same relaxation time. The critical exponents which enter into the LK contribution are those of mean-field theory. Critical-exponent values for other universality classes, particularly for the 3D Ising model, are found to be inconsistent with the data.

Above the N -IC transition temperature T_i , the acoustic anomalies are explained by the coupling of the longitudinal-acoustic mode to fluctuations in the energy density associated with the soft mode. These fluctuations can be accounted for using dynamic scaling theory. The data are not sufficient to determine quantitatively the values of the critical exponents which enter into the theory, but the data are seen to be consistent with 3D Ising-model values of the exponents.

ACKNOWLEDGMENTS

We wish to thank Professor R. Laiho and Professor Y. Ishibashi for making their data available to us, and Professor Carl Garland for helpful discussions and suggestions. This work was supported in part by NSF Grant No. DMR-9002279 and by contributions from DuPont, Perkin-Elmer, and the Alfred P. Sloan Foundation.

- ¹J. D. Axe, M. Iizumi, and G. Shirane, in *Incommensurate Phases in Dielectrics: Materials*, edited by R. Blinc and A. P. Levanyuk (North-Holland, Amsterdam, 1986), pp. 1–48.
- ²K. Gesi and M. Iizumi, *J. Phys. Soc. Jpn. Lett.* **48**, 337 (1980).
- ³J. Henocque, J. L. Sauvajol, J. Lefebvre, and G. Marion, *J. Raman Spectrosc.* **14**, 93 (1983).
- ⁴J. Berger, J. P. Benoit, C. W. Garland, and P. W. Wallace, *J. Phys. (Paris)* **47**, 483 (1986).
- ⁵H. Hoshizaki, A. Sawada, and Y. Ishibashi, *J. Phys. Soc. Jpn.* **47**, 341 (1979).
- ⁶J. Berger and J. P. Benoit, *Solid State Commun.* **49**, 541 (1984).
- ⁷E. Käräjämäki, R. Laiho, and T. Levola, *J. Phys. C* **16**, 6531 (1983).
- ⁸L.-T. Cheng and K. A. Nelson, *Phys. Rev. B* **39**, 9437 (1989).
- ⁹L.-T. Cheng and K. A. Nelson, *Phys. Rev. B* **37**, 3603 (1988).
- ¹⁰M. R. Farrar, L.-T. Cheng, Y.-X. Yan, and K. A. Nelson, *IEEE J. Quantum Electron* **QE-22**, 1453 (1986).
- ¹¹Y.-X. Yan and K. A. Nelson, *J. Chem. Phys.* **87**, 6240 (1987); **87**, 6257 (1987).
- ¹²S. M. Silence, S. R. Goates, and K. A. Nelson, *Chem. Phys.* **149**, 233 (1990).
- ¹³H. Z. Cummins, *Phys. Rep.* **185**, 211 (1990).
- ¹⁴H. J. Eichler, P. Gunter, and D. W. Pohl, *Laser-Induced Dynamic Gratings* (Springer, Berlin, 1986); K. A. Nelson and M. D. Fayer, *J. Chem. Phys.* **72**, 5205 (1980); K. A. Nelson, D. R. Lutz, M. D. Fayer, and L. Madison, *Phys. Rev. B* **24**, 3261 (1981).
- ¹⁵J. Hu, J. O. Fossum, C. W. Garland, and P. W. Wallace, *Phys. Rev. B* **33**, 6331 (1986).
- ¹⁶Z. Hu, C. W. Garland, and S. Hirotsu, *Phys. Rev. B* **42**, 8305 (1990).
- ¹⁷S. Hirotsu, K. Toyota, and K. Hamano, *Ferroelectrics* **36**, 319 (1981).
- ¹⁸J. O. Fossum, *J. Phys. C* **18**, 5331 (1985).
- ¹⁹R. A. Cowley and A. D. Bruce, *J. Phys. C* **11**, 3577 (1978).
- ²⁰R. D. Williams and I. Rudnick, *Phys. Rev. Lett.* **25**, 276 (1970).
- ²¹R. Blinc, D. C. Ailion, J. Dolinsek, and S. Zumer, *Phys. Rev. Lett.* **54**, 79 (1985).
- ²²T. P. Dougherty, G. P. Wiederrecht, and K. A. Nelson (unpublished).
- ²³T. P. Dougherty, G. P. Wiederrecht, M. H. Garrett, and K. A. Nelson (unpublished).